PCCP

Explosion limits of hydrogen-oxygen mixtures from nonequilibrium critical points

Journal:	*Physical Chemistry Chemical Physics*
Manuscript ID	CP-ART-02-2018-000905.R2
Article Type:	Paper
Date Submitted by the Author:	18-May-2018
Complete List of Authors:	Newcomb, Lucas; University of Massachusetts Boston, Chemistry Marucci, Michael; University of Massachusetts Boston, Chemistry Green, Jason; University of Massachusetts Boston, Chemistry

Explosion limits of hydrogen-oxygen mixtures from nonequilibrium critical points

Lucas B. Newcomb,[1] Michael E. Marucci,[1] and Jason R. Green[1, 2, 3, *]

[1] *Department of Chemistry, University of Massachusetts Boston, Boston, MA 02125*
[2] *Department of Physics, University of Massachusetts Boston, Boston, MA 02125*
[3] *Center for Quantum and Nonequilibrium Systems, University of Massachusetts Boston, Boston, MA 02125*

The explosion limits of hydrogen-oxygen mixtures are macroscopic, temperature-pressure boundaries that divide the overall chemistry of hydrogen oxidation into slow-burning and explosive regimes. Here, we demonstrate that it is possible to recover the three chemical explosion limits of H_2/O_2 mixtures from nonequilibrium stochastic trajectories. This demonstration relies on the finding that, in explosive regimes, these trajectories have the quantitative features of a dynamical phase transition. Through computer simulations for both a generic and a reduced model for hydrogen oxidation, we find only one dominant reactive phase at temperatures below the explosion limits. At temperatures above the limits, however, a second phase transiently emerges from the chemistry. By locating the pseudo-critical temperature where two reactive phases are distinguishable, we construct all three explosion-limit boundaries for model hydrogen-oxygen mixtures of finite size.

Keywords: ignition — phase transitions — nonequilibrium statistical mechanics

I. INTRODUCTION

Hydrogen combustion is of practical importance in applications that include space exploration[1] and renewable energy.[2] The chemically-driven phenomena that underlie these applications are also relevant to the efficient combustion and safe storage of hydrogen.[1–5] Hydrogen is an appealing source of power because of its high energy density and cleanliness compared to petroleum-based fuels.[6] Moreover, the chemistry of hydrogen oxidation plays a role in the combustion of other fuels.[7] Much progress has been made in the fundamental understanding of the behavior of hydrogen-oxidizer mixtures, particularly at a bulk level of description.[8–10] However, without a fully developed theory of nonequilibrium statistical mechanics,[11] it is less clear how the microscopic dynamics of combustion chemistry translates into bulk behavior.

It has long been known that the chemistry of hydrogen oxidation depends strongly on pressure, temperature, and mixture composition.[8] How thermodynamic variables control the kinetic and thermal feedback mechanisms underlying ignition is grounded in the "explosion limits".[8–10,12,13] Below these limits, H_2/O_2 mixtures experience a steady, slow burn. However, mixtures explode upon crossing these boundaries. In the latter regime, the pool of radicals proliferates and facilitates further decomposition of fuel and oxidizer. The characteristic chemicals that proliferate during explosions are the intermediate species (H, O, OH, H_2O_2 and HO_2), which lead to water. For hydrogen, the explosion limits have a characteristic "Z-shape" structure in the space of temperature and pressure.[9,10,14] Traveling from low to high pressure, the individual branches of the "Z" constitute the first, second, and third explosion limits, respectively: each having their own, unique dominant reactions.

Crossing an explosion limit takes only a small change in a thermodynamic field but has a large effect on reactive behavior and heat release – a response reminiscent of phase transitions.[15,16] By imposing constant temperature, which eliminates the contribution of reaction heat release during combustion, we have previously demonstrated that chemical explosions of H_2/O_2 mixtures have (1) the quantitative features of a first-order dynamical phase transition above the second explosion limit and (2) that the critical temperature, below which ignition does not occur, converges to the second explosion limit temperature for sufficiently large systems at one atmosphere.[17] Although explosions necessarily generate heat, several works have shown that purely chemical feedback mechanisms can produce three explosion limit boundaries.[6,14,18] Here, we test the hypothesis that all points on these boundaries are critical points with two models for hydrogen combustion: one model based on a reduced set of elementary reactions and another (generic) model that captures some of the essential chemical processes.[14]

Over a range of temperatures and pressures, we simulate many trajectories of a reacting H_2/O_2 system, each trajectory being a realization of the solution to the chemical master equation. We then show that ignition is a transient, dynamical phase transition[19,20] using trajectory observables. The results are evidence that previous findings are not unique to the reduced model used or the second explosion limit.[17] Here, after detailing the models and methods, we demonstrate an ability to map the "Z-shaped" explosion limits for two model mechanisms: evidence suggesting that macroscopic explosion limits are a family of nonequilibrium critical points. Looking ahead, if other igniting, fuel-oxidizer mixtures exhibit this phase behavior, then the approach we introduce here is a means of translating the microscopic chemical events of combustion chemistry into macroscopic explosion limits.

* jason.green@umb.edu

II. MODELS AND SIMULATION METHODS

Fluctuations in the concentration of intermediates can stimulate ignition, so we simulate the stochastic evolution of reacting mixtures to investigate the underlying microscopic causes of explosion limits.[21–23] By explicitly accounting for fluctuations of intermediate species, this approach differs from traditional chemical kinetic modeling,[12,14,24,25] which is based on mean-field rate equations. As a proof-of-principle, we simulate the stochastic chemistry of two models for hydrogen combustion: (1) a reduced set of elementary H_2/O_2 reactions and (2) a symbolic set of elementary steps.[14] Previous works demonstrated that these, and other, reduced mechanisms have three explosion limits.[6,7,14,26,27] Since the explosion limits of these mechanisms are known in the macroscopic limit, they can serve as a benchmark to test the hypothesis that all three limits exhibit the features of a nonequilibrium phase transition.

A. Stochastic simulations of hydrogen oxidation

We model the stochastic time evolution of a finite number of reactant molecules with Gillespie's exact stochastic algorithm.[21–23] All systems are initially composed of only reactants (H_2/O_2 or R) in their stoichiometric ratios and evolve towards a final state dominated by the product (H_2O or P). For each temperature-pressure point simulated, we evolve a minimum of 10^6 trajectories. Along the nonequilibrium pathway to the steady-state, intermediates are born and destroyed by initiation, propagation, branching, and termination. To select the sequence of reactions, each elementary step is given a propensity, a_i. Bimolecular reactions with chemically distinct reactants have a propensity of $k_i X_1 X_2/N_a V$. For termolecular reactions, the propensity is $k_i X_1 X_2 X_3/N_a^2 V^2$ when the reactants are chemically distinct and $k_i X_1 X_2 (X_2 - 1)/2N_a^2 V^2$ when two reactants are identical: the factor $X(X-1)/2$ avoids overcounting reaction pairs.[21,22] In all cases, the propensity has units of inverse time. Here, N_a is Avogadro's number, V is the volume, and k_i is the rate coefficient for the ith reaction.

The propensities are used to determine reaction probabilities, $a_i/\sum_m a_m$. A uniform random number determines which reaction occurs, the system composition is updated by the stoichiometry of the selected reaction, and time is updated ($t_{k+1} = t_k + \tau$) by the time between reactions, $\tau = -\left(\sum_m a_m\right)^{-1} \ln x$ with $x \in [0,1]$. Since the rate coefficients for the symbolic model have no units of time, we divide the time between reactions by the smallest rate constant such that both timescales are unitless to facilitate a comparison of the results for each model. The slowest reaction in both models is initiation, so we use the scaled time $t/\tau_{\max}$ with $\tau_{\max} = 1/k_{\text{initation}}$ for both models.

B. Reduced model for hydrogen oxidation

The reduced model[14] we use to simulate the overall reaction $2H_2 + O_2 \rightarrow 2H_2O$ has seven irreversible reactions:

$$\begin{aligned}
H_2 + O_2 &\xrightarrow{k_1} H + HO_2 && (R_1)\\
H + O_2 &\xrightarrow{k_2} O + OH && (R_2)\\
O + H_2 &\xrightarrow{k_3} H + OH && (R_3)\\
H_2 + OH &\xrightarrow{k_4} H + H_2O && (R_4)\\
H + O_2 + M &\xrightarrow{k_5} HO_2 + M && (R_5)\\
HO_2 + H_2 &\xrightarrow{k_6} H_2O_2 + H && (R_6)\\
H_2O_2 + M &\xrightarrow{k_7} 2\,OH + M. && (R_7)
\end{aligned}$$

Initiation of a radical carrying chain, through R_1, provides the initial radical(s) needed for ignition. Reactions 2 and 3 are low to medium pressure branching reactions and are important to the first and second explosion limits. Reaction 4 is the chain propagation step and the only reaction that produces water. The gas-phase (nominal) termination step, R_5, is mainly responsible for suppressing ignition near the second limit. At high pressure, R_6 can feed directly into R_7 and sustain branching. Because these last two reactions require sufficiently high pressure to occur, they become significant in the kinetics at the third limit.

In this mechanism, the species M represents any gas-phase collision partner. We approximate the concentration, [M], with the ideal gas law, p/RT.[28] All systems begin as a stoichiometric mixture of H_2 and O_2. As is common in the combustion literature,[6,9,14,18,23,27] the rate coefficient, k_i, for the ith gas-phase reaction is calculated using the modified Arrhenius equation,

$$k_i(T) = A_i T^{\delta_i} e^{-E_{a,i}/RT}, \qquad (1)$$

where A_i is the pre-exponential factor, T is the temperature in Kelvin, δ_i is the temperature-dependence exponent, $E_{a,i}$ is the activation energy, and R is the molar gas constant. To model the dependence of reactions R_5 and R_7 on pressure, we use the Lindemann form: $k_i = [\mathrm{M}]^{-1}\left(1/k_\infty + 1/k_0[\mathrm{M}]\right)^{-1}$, where the subscripts indicate infinitely high and zero pressure limits of k_i. Additionally, we treat all third-body species as having the same enhancement coefficient.

We model the wall termination of H and HO_2 with rate constants that depend on the features of the reaction vessel,

$$k_{\text{wall}} = \frac{1}{4}\epsilon\bar{\nu}\frac{S}{V}, \qquad (2)$$

including the fraction of wall collisions that successfully terminate the radical, ϵ, known as the "sticking coefficient". We take the value of ϵ to be 10^{-3} for H and 3×10^{-3} for HO_2. Here, $\bar{\nu}$ is the average thermal velocity of gas-phase molecules given by $\sqrt{8k_BT/\pi M_m}$, where k_B is the Boltzmann constant, T is the temperature in

Kelvin, and M_m is the molar mass of the terminating species. The propensity of wall termination reactions is taken to be $k_{\text{wall}}X_j$. We model our system as a spherical container with a surface area to volume ratio, S/V, of $3/r$ and a fixed radius, r, of 0.074 cm. We only include the wall termination of H and HO_2 because, as was shown previously for this model,[14] the destruction of these species is sufficient to suppress the chain-branching and give the first and third limits, respectively.

While our aim is to test the hypothesis that the entire Z-shaped explosion boundary is composed of nonequilibrium critical points, the accuracy of the third explosion limit, in particular, requires further comment. It is well-known that the third limit is highly sensitive to the elementary reactions in the model; namely, those involving HO_2 and H_2O_2, as we have seen in molecular dynamics simulations.[29] It has been discussed recently that the models here, and the Lindemann form of the pressure dependence of the rate-constants for R_5 and R_7, reduce the accuracy of the explosion limits.[6,14,27,30] As is commonly done in deriving explosion limits from mass-action rate equations, our simulations neglect heat release, which can also affect the location of the third explosion limit, and treat systems as well-mixed. These conditions, however, do not invalidate the proof-of-principle that explosion limits emerge – and can be extracted – from stochastic trajectories without mass-action rate equations.

C. Symbolic model for hydrogen oxidation

The second model[14] we consider is a symbolic model that consists of six irreversible reactions:

$$\begin{aligned}
2\,\mathrm{R} &\xrightarrow{k_1'} \mathrm{C} && (\mathrm{R}_1')\\
\mathrm{C}+\mathrm{R} &\xrightarrow{k_2'} 2\,\mathrm{C}+\mathrm{P} && (\mathrm{R}_2')\\
\mathrm{C}+2\,\mathrm{R} &\xrightarrow{k_3'} \mathrm{D}+\mathrm{R} && (\mathrm{R}_3')\\
\mathrm{D}+\mathrm{R} &\xrightarrow{k_4'} 2\,\mathrm{C}+\mathrm{P} && (\mathrm{R}_4')\\
\mathrm{C} &\xrightarrow{k_5'} \mathrm{P} && (\mathrm{R}_5')\\
\mathrm{D} &\xrightarrow{k_6'} \mathrm{P}. && (\mathrm{R}_6')
\end{aligned}$$

The species R represents the reactants (e.g., H_2 and O_2), C and D are the low and high pressure radical chain carriers (representing H, H_2O_2, and HO_2), and P is the stable product analogous to H_2O. Reaction 1 is the chain initiation step, which generates the first radical needed to begin the branching process. Reaction 2 is the low-pressure branching reaction, and Reaction 3 is the corresponding gas-phase termination of the low pressure radical, C. Reaction 4 represents the high pressure branching step for the termination product of Reaction 3; branching from species D only occurs at high pressures, so at intermediate and low pressures, it is preferentially terminated on the wall. Reactions 5 and 6 are the wall termination reactions for C and D, which are important in the first and third explosions limits, respectively.

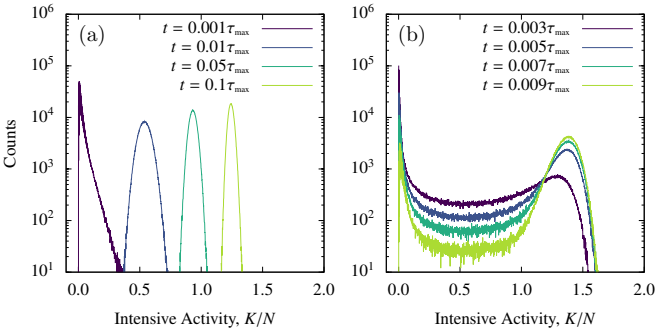

FIG. 1. Histograms of intensive activity for the symbolic model at a pressure of 100 Pascals and a temperature of (a) 740 Kelvin, below the explosion temperature, and (b) 760 Kelvin, above the explosion temperature. All histograms are from a sample of 10^6 trajectories. In (a), the distribution initially peaks at low activity and remains unimodal as time progresses. In (b), the distribution still initially peaks at a low activity but is transiently bimodal with equal peak heights at t^*. Both models exhibit the qualitative behavior illustrated by these histograms (with different temperatures and pressures marking the onset of bimodality).

Following Ref. [14], the rate coefficients for each reaction are: $k_1' = 10^{-6}$, $k_2' = 10^5 e^{-9000/T}$, $k_3' = 1.0$, $k_4' = 10^5 e^{-16000/T}$, and $k_5' = k_6' = 0.01$, where T is the temperature in Kelvin. Note that the second and fourth rate constants are in a modified Arrhenius form to model their temperature dependence. This form differs slightly from the traditional equation because the numerator inside the exponent is not an activation energy but rather an activation temperature with units of Kelvin. We do not use the Lindemann equation to account for the pressure dependence of the symbolic reaction rate coefficients. However, the propensities are pressure dependent through the volume term in the propensity for bimolecular and termolecular reactions. Reaction R_3', for example, is termolecular and its propensity is proportional to the square of the pressure. The propensities of bimolecular reactions vary linearly with pressure.

III. RESULTS AND DISCUSSION

A. Bimodality of trajectory observables

During each trajectory, the initial reactants are turned into intermediate chain carriers that terminate to form product(s). To characterize these dynamical histories through the space of compositions, we use the dynamical activity, K. We define $K = K[\mathbf{x}(t_{\text{obs}})]$ as the number of reactions occurring in a mixture of N molecules (initially) at a pressure p and temperature T over an observation time $0 \le t \le t_{\text{obs}}$, $K[\mathbf{x}(t_{\text{obs}})] = \sum_i \mathbb{1}(\Delta t_i)$. The indicator function $\mathbb{1}(\Delta t_i) = 1$ if a reaction event occurs and is zero otherwise. We divide t_{obs} uniformly into intervals, Δt, apply the indicator function in each, and sum over time

intervals to get the activity. In the transient combustion reaction, the activity is not extensive in time; the activity grows over the course of a trajectory but reaches a fixed value when the reaction is complete. This behavior is also found in other irreversible hydrogen combustion mechanisms.[17]

The temporal behavior of the activity reflects the underlying chemistry and, so, depends on whether the macroscopic conditions are above or below the explosion limits. Below the explosion limits, intermediates terminate soon after forming; the temporal profile of the cumulative number of reactions – the activity, K – tends to steadily increase in most trajectories until the reaction is complete. The activity tends to grow more rapidly at higher temperatures and pressures. Above the limits, some intermediates (e.g., the radicals H, OH and HO_2) accumulate in significant quantities: the peak amounts, specifically, are dependent on pressure and temperature. Because of the proliferation of radicals, the activity undergoes a rapid jump, indicating an (auto)ignition event. By the end of the trajectories, the product(s) dominate the mixture, reactions cease, and the activity plateaus.

The ensemble of trajectories characterizes the overall reaction. From our sample of this ensemble, we find the histograms of the activity are also dramatically different above and below the explosion limits, as shown in Fig. 1. Below the explosion limits, there is a single peak in the activity distribution consistent with the slow burning of the mixture and the absence of ignition, Fig. 1a. Above the explosion limits, however, the trajectory ensemble exhibits the signatures of a transient dynamical phase transition. These signatures appear in the integrated activity of all the trajectories between 600 and 1000 Kelvin and 10^1 to $2{\times}10^6$ Pascals for both the reduced model and the symbolic model. Above the three explosion limits, a prominent feature of the activity distribution is the transient coexistence of two peaks. We denote the time that these peak heights are equal as t^*, Fig. 1b. At times before or after t^*, the distribution may be unimodal. In contrast, trajectory ensembles at temperature and pressure outside the explosive conditions never display bimodality at any time.

B. Coexistence of autoigniting and non-igniting dynamical phases

We assign the trajectories associated with the two peaks in the activity distribution to a dynamical phase. Each phase corresponds roughly to the progress of the overall reaction exhibited in that phase: there is an autoigniting "active" phase associated with the maximal peak height at $K_a = N\kappa_a$ and a slow burning "inactive" phase associated with the lower activity peak at $K_i = N\kappa_i$. Here, κ_i and κ_a are the most probable activity density (activity per molecule) for the active and inactive phases. These two peaks in the activity distribution reflect the transient bi-stability and coexistence

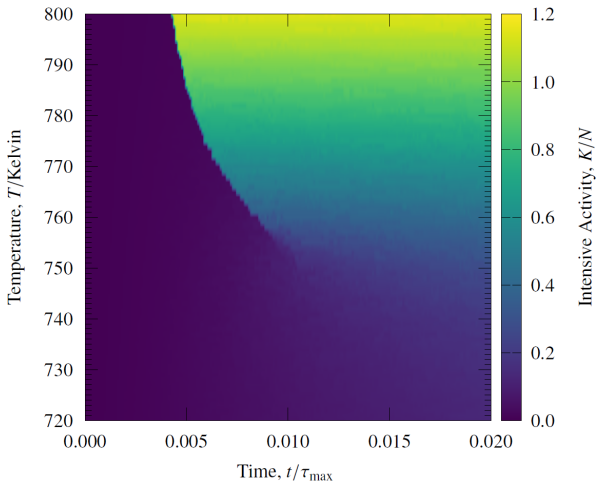

FIG. 2. Representative dynamical phase diagram for temperatures near the first explosion limit for the symbolic hydrogen model at 100 Pascals ($N = 10^3$ molecules initially). The sharp boundary marks the coexistence of the inactive and active phases at the characteristic time t^* when the inactive and active peaks heights are equal. For a given pressure, the pseudo-critical temperature (and time) is where the active and inactive peaks are indistinguishable (approximately 750 Kelvin). The pseudo-critical temperatures coincide with the explosion limit temperatures for each pressure. The reduced model has a qualitatively similar phase diagram (not shown).

of two dynamical phases. A map of the coexistence of these phases or "dynamical phase diagram" is shown in Fig. 2 for conditions near the first explosion limit for the symbolic model.

To understand the origin of the bistability, we separately analyze the high and low activity trajectories. First, each dynamical phase has a distinct composition of chemical species and reactions for both models. For example, mixtures at t^* that reside in low activity trajectories are largely composed of reactants, H_2/O_2 or R. High activity trajectories, however, are composed mostly of products, H_2O or P. Second, the mole fractions of each species in the active and inactive trajectories reflect the frequency of reactions and overall progress of the reaction. The low activity (inactive phase) trajectories are dominated by termination reactions (R_5, wall terminations, R_3', R_5', and R_6') that annihilate radicals, while the high activity (active phase) trajectories are dominated by branching reactions (R_3, R_4, R_6, R_7, R_2', and R_4') that create radicals and water.

The unique time t^* at which dynamical phases coexist depends strongly on pressure and temperature. Using temperature, pressure, and time as control variables, we map the most probable activity per molecule, K/N. The resulting phase diagram in Fig. 2 shows a jump from κ_i to κ_a in the most probable activity per molecule at t^*. Because the long-time limit of the activity is linearly extensive in the number of molecules, the density K/N has an approximate range of $[0, 2.0]$. Just above the phase

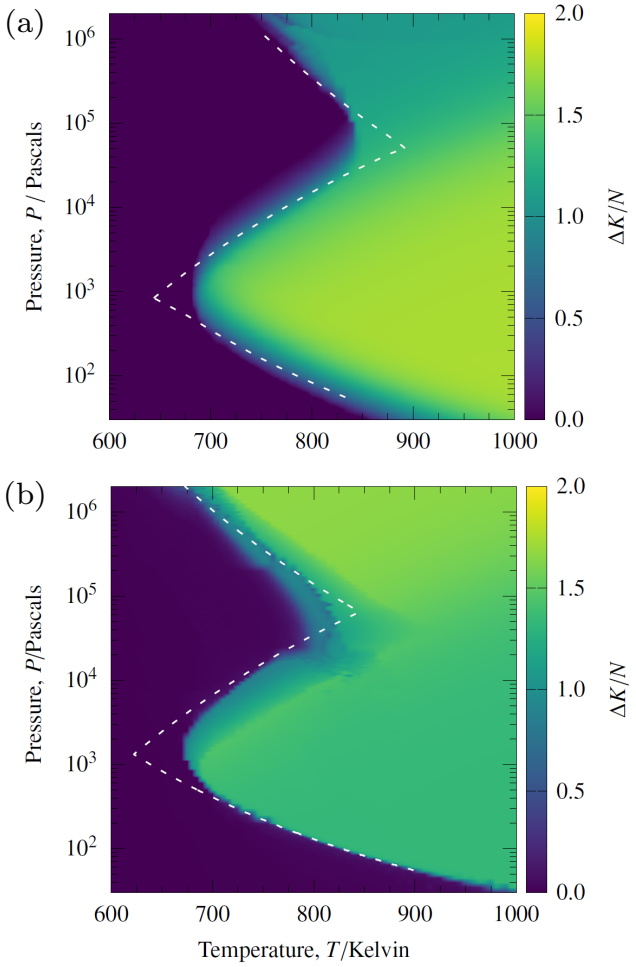

FIG. 3. A map of $\Delta K/N$ at t^* in temperature-pressure space shows the "Z-shaped" explosion limits for the (a) symbolic and (b) reduced models. On the high temperature side of the explosion boundary, two dynamical phases will coexist transiently. For a given pressure, the lowest temperature with a measurable difference between activity peak heights, $\Delta K/N = \kappa_a - \kappa_i$, is approximately the pseudo-critical temperature, $T_c(N)$. Over the range of pressures here, the family of pseudo-critical temperatures agrees well with the asymptotic explosion limits (dashed lines) and marks the thermodynamic conditions where mixtures can ignite.

boundary, >95% of trajectories are in the active phase, and just below the boundary, >95% of trajectories are in the inactive phase. Crossing the coexistence boundary by increasing time or temperature causes a switch in the most abundant dynamical phase from inactive to active.

Along the phase boundary, the active and inactive peaks are of equal height. A similar diagram results, however, using the "equal area rule".[31] Moving along the coexistence line in the direction of increasing time, the distance between the peak heights, $\Delta K = K_a - K_i$ at t^* measures the activity change that accompanies the sudden burst of reactions upon ignition. We show the separation between activity peaks in Fig. 3 for the two models across all simulated T and p. This quantity measures the "latent activity" associated with the transformation of a gaseous mixture over a small time window. The magnitude of ΔK depends on the dominant reactive pathway, unique to each model and, within the model, depends on the reactions taking place at each limit. In essence, ΔK is a measure of the difference in the progress of the overall reaction between the inactive and active trajectories.

The magnitude of ΔK is zero when only one peak exists in the temporal profile of the activity; otherwise, there is a second activity peak and $\Delta K > 0$. The difference in activity ΔK between the two phases shrinks moving down the coexistence line. Ultimately, $\Delta K \to 0$ and vanishes at the pseudo-critical point, the time-temperature point corresponding to the loss of bimodality in the activity distribution. The temperature corresponds to the previously reported explosion limit temperature for both of these models.[14] From a visual inspection of the reaction counts, trajectories below the critical point exhibit reaction patterns with repeated initiation and termination, which prevents sustained branching and the growth of the radical pool. Above the critical temperature at a given pressure, the evolution of trajectories transitions from repeated initiation and termination to having periods of sustained branching and propagation. The low activity trajectories have a long ignition delay as a result of frequent termination reactions and the high activity trajectories undergo a large jump in activity over a short amount of time as a result of sustained branching.

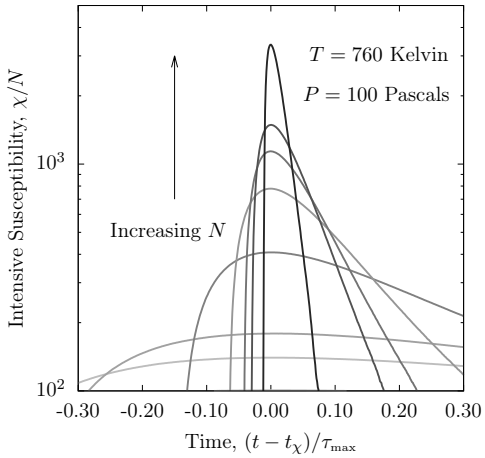

FIG. 4. The intensive susceptibility, $\chi(t)/N$, as a function of time. Data shown are for 10^6 trajectories above the explosion limit at 100 Pascals and 760 Kelvin for the symbolic model; these data are representative of the behavior of both models above their respective explosion limits. The susceptibility concentrates around t_χ upon increasing the initial number of molecules, N, in the mixture. The scaling of the statistical parameters of these data, such as the height and temporal location of the peak, correspond to those of a first-order phase transition above the explosion limit. For example, the maximum susceptibility scales as $\mathcal{O}(N^2)$ above the explosion limit and as $\mathcal{O}(N)$ below.

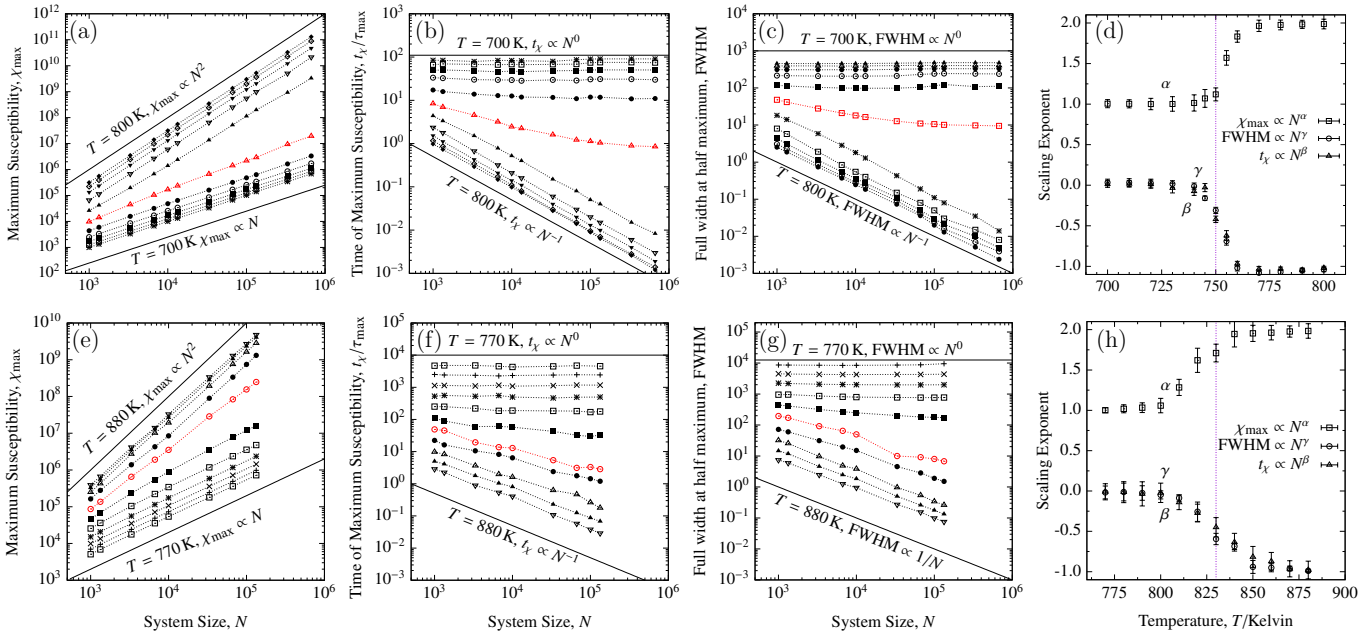

FIG. 5. Scaling of the susceptibility, $\chi(t, N)$, with the initial number of molecules (N, system size) for the symbolic (a-d) and reduced (e-h) models near the first explosion limit. The scaling of (a,e) the maximum susceptibility, (b,f) the temporal location of the maximum susceptibility, and (c,g) the full width of the susceptibility at half the maximum. The scaling behavior of these observables changes abruptly across the explosion temperature at 100 Pascals: 750 K for the symbolic model and 830 K for the reduced model; the scaling above the explosion limit is consistent with a first-order dynamical phase transition at t^* and T^* above $T_c(N)$. The scaling exponents exhibit a crossover (d) at 750 K for the symbolic and (h) at 830 K for the reduced model. These crossover temperatures are consistent with previously reported explosion limits at the first limit.[14]

The main result here is that the temperatures and pressures where ΔK becomes nonzero correspond to the points on all three explosion limits for both the reduced hydrogen and symbolic models. This result is apparent in Fig 3, which shows $\Delta K/N$ for ensembles of trajectories over a range of temperature and pressure. It is clear that these maps have the well-known "Z-shaped". For comparison, the asymptotic explosion limits are also shown (dashed lines). They are conditions where the rates of radical proliferation and termination are in balance. These macroscopic limits derive from the rate constants for the key elementary reactions at each limit. For example, the asymptotic line for the second limit in the reduced model is when $2k_2/k_5 = [\mathrm{M}]$. When the rate of radical branching through R_2 is greater than its termination through R_5, the system will explode at intermediate pressures.[14] The asymptotic limits for the symbolic model are k_5'/k_2', k_2'/k_4', and k_2'/k_3' for the first, second, and third limits, respectively. For the reduced mechanism, these limits are k_H/k_2, $2k_2/k_5$, k_{HO_2}/k_6, where k_{HO_2} and k_H are the rate coefficients for the wall termination reactions. The data in Fig 3 show that for both models the boundaries identified through stochastic simulations compare well to these asymptotic boundaries. They also show that, while reactions in the symbolic model do not have a Lindemann pressure dependence, both models are in qualitative agreement with each other and have three explosion boundaries.

C. Finite-size scaling of activity fluctuations

As further evidence that explosion limits are dynamical phase transitions, we analyze the finite-size scaling of activity fluctuations.[31,32] For all systems, we analyze the variance of the activity or susceptibility, $\chi(t, N) = \langle K^2 \rangle - \langle K \rangle^2$, where $\langle \ldots \rangle$ indicates an average over trajectories. The evolution of the susceptibility over time depends on whether the temperature and pressure are above or below the explosion limit. Above the explosion limit, for example, the susceptibility in activity evolves from zero (at the start of the reaction) through a maximum value (during ignition) before decaying to a fixed value at long times (Fig. 4).

Several features of this peak in the susceptibility characterize the dynamical phase transition: the maximum susceptibility, time of maximum susceptibility, and the full width at half maximum (FWHM). The scaling of these features indicates whether there is one phase or two coexisting phases. Fig. 5 shows their dependence on system size, N, for temperatures above and below the explosion temperatures for both models at 100 Pascals in system sizes ranging from $N = 10^3$ to 10^6. As a function of N and temperature, the maximum susceptibility has a linear dependence on N, $\chi_{max} = \mathcal{O}(N)$ below the explosion temperature. This scaling is consistent with the existence of a single phase and the unimodality of the activity distribution. However, upon crossing

the explosion temperature, the maximum susceptibility becomes proportional to the square of the system size, $\chi_{\max} = \mathcal{O}(N^2)$, indicating bimodality and the coexistence of two phases. Above the explosion temperature, the time of max susceptibility, t_χ and the FWHM show the scaling we expect for a first order phase transition, analogous to that of water along the liquid-vapor coexistence line: the time of max susceptibility and the FWHM transition from being proportional to N^0 below the critical temperature to N^{-1} above.

Fig. 5d shows the scaling exponent of these observables versus temperature to show their non-linear dependence on N upon passing through the critical point. Interestingly, the crossover in the finite-size scaling exponents is not particularly sharp. We also note that the scaling exponents of the symbolic model crossover more quickly across the explosion limits than the scaling exponents of the reduced model, which change slowly for t_χ and FWHM. We have also analyzed the finite-size scaling for another reduced model of hydrogen oxidation near the second explosion limit.[17] From these three models, it appears the crossover sharpness depends on the model and that models with fewer competing reactions seem to produce a sharper crossover. This effect could be statistical in origin, since models with fewer possible reaction paths must necessarily have less variation in their composition of reactions. More work is necessary to establish this observation, however.

The model here, and the nonequilibrium phase transition it exhibits, is similar to the branching process[33] in that it lacks spatial degrees of freedom and, therefore, does not have a correlation length.[34] At equilibrium, there are quantities that diverge at the critical point. In these zero-dimensional models for hydrogen combustion, while there is no correlation length, the branching time does diverge. At the explosion limits, the characteristic branching time diverges because $t_B = 1/(k_3 - k_5[\mathrm{M}])$. The denominator here is the condition for the asymptotic explosion limits, which must be equal to zero along the asymptotic lines.[8,14] Since the characteristic time to produce radicals diverges, it is then reasonable to expect that the ignition-delay time would also diverge as a result of the balance of branching and termination rates at the asymptotic explosion limits.[35]

IV. CONCLUSIONS

To summarize, the trajectory ensembles of reacting hydrogen systems exhibits two dynamical phases at and above all three of the explosion limits of two models for chemically-driven explosions; below these limits, the trajectory ensemble has a unimodal activity distribution. The coexistence of these two phases and the scaling of the activity fluctuations above the critical temperature and pressure show that the dynamical phase transition is first order. From the temperature-time dynamical phase diagrams, the coexistence of these two phases terminates at a pseudo-critical point – the lowest temperature where these phases are distinguishable. The family of these critical points over a range of pressure is the well-known "Z-shaped" explosion diagram known for hydrogen combustion in chemical kinetics. It remains to be seen whether explosion limits of other fuels might also be recovered through this methodology. Looking ahead, it would also be of interest to model the energy released as heat during the reaction and increase the accuracy of the third explosion limit predicted by the models we adopted here. Furthermore, the method of mapping explosion limit boundaries from nonequilibrium pseudo-critical points is independent of the commonly used mass-action rate theories and so, in principle, could lead to the determination of explosion boundaries from molecular dynamics simulations.[29]

V. ACKNOWLEDGEMENTS

This material is based upon work supported by the U.S. Army Research Laboratory and the U.S. Army Research Office under grant number W911NF-14-1-0359. We acknowledge the use of the supercomputing facilities managed by the Research Computing Group at the University of Massachusetts Boston as well as the University of Massachusetts Green High Performance Computing Cluster. L.B.N. acknowledges the Oracle Education Foundation for a Doctoral Research Fellowship. The authors thank Dr. Moupriya Das and Rebecca A. Bone for comments on the manuscript.

[1] V. Dawson and M. Bowles, *Taming Liquid Hydrogen: The Centaur Upper Stage Rocket* (National Aeronautics and Space Administration, 2004).
[2] T. W. S. Verhelst, Progress in Energy and Combustion Science **35**, 490527 (2009).
[3] C. M. White, R. R. Steeper, and A. E. Lutz, Int. J. of Hydrogen Energy **31**, 1292 (2005).
[4] I. Ray, T. Chakraborty, D. Roy, A. Datta, and B. K. Mandal, Intl. J. of Emerging Tech. and Adv. Eng. **3**, 119 (2013).
[5] S. Verhelst, Int. J. of Hydrogen Energy **39**, 1071 (2014).
[6] A. L. Sànchez and F. A. Williams, Progess in Energy and Combustion Science **41**, 1 (2014).
[7] P. Boivin, A. L. Sànchez, and F. A. Williams, Combustion and Flame **176**, 489 (2017).
[8] B. Lewis and G. V. Elbe, *Combustion, Flames and Explosions of Gases*, 3rd ed. (Academic Press, 1987).
[9] I. Glassman and R. A. Yetter, *Combustion* (Elsevier, San Diego, CA, 2008).
[10] C. K. Law, *Combustion Physics*, 1st ed. (Cambridge University Press, Cambridge, 2006).
[11] C. Jarzynski, Nat. Phys. **11**, 105 (2015).

[12] N. N. Smirov and V. F. Nikitin., Int. J. of Hydrogen Energy **39**, 987 (2013).
[13] G. Y. Gerasimov and O. P. Shatalov, J. of Eng. Phys. and Thermophysics **86(5)**, 987 (2013).
[14] X. Wang and C. K. Law, J. Chem. Phys. **138**, 134305 (2013).
[15] N. Goldenfeld, *Lectures on phase transitions and the renormalization group*, 1st ed. (Westview Press, 1992).
[16] J. M. Yeomans, *Statistical mechanics of phase transitions*, 1st ed. (Clarendon Press, 1992).
[17] L. B. Newcomb, M. Alaghemandi, and J. R. Green, J. Chem. Phys. **147**, 1 (2017).
[18] C. K. Law, *Combustion Physics*, 1st ed. (Cambridge University Press, 2006).
[19] H. Hinrichsen, Adv. Phys. **49**, 815 (2000).
[20] G. Nicolis, NATO ASI **120**, 171 (1983).
[21] D. T. Gillespie, J. Phys. Chem **81**, 2340 (1977).
[22] D. T. Gillespie, Physica A **188**, 404 (1992).
[23] D. G. Vlachos, Chemical Engineering Science **53**, 157 (1996).
[24] "CHEMKIN-PRO 15131, Reaction Design: San Diego," (2013).
[25] A. L. Sánchez, E. Fernández-Tarrazo, P. Bovin, A. L. nan, and F. A. Williams, C.R. Mecanique **340**, 882 (2012).
[26] P. Bovin, C. Jimé, A. L. Sánchez, and F. A. Williams, International Symposium on Combustion **33**, 1 (2010).
[27] A. L. Sànchez, E. Fernàndez-Tarrazo, and F. A. Williams, Combustion and Flame **161**, 111 (2013).
[28] U. Maas and J. Warnatz, .
[29] M. Alaghemandi, L. B. Newcomb, and J. R. Green, J. Phys. Chem. A **121**, 1686 (2017).
[30] M. P. Burke, M. Chaos, Y. Ju, F. L. Dryer, and S. J. Klippenstein, Int. J. Chem. Kin. **44**, 444 (2011).
[31] C. Borgs and R. Kotecký, J. Stat. Phys. **61**, 79 (1990).
[32] K. Binder and D. P. Landau, Phys. Rev. B **30**, 1477 (1984).
[33] V. Privman, *Nonequilibrium statistical mechanics in one dimension* (Cambridge Univeristy Press, Cambridge, MA, 1997).
[34] J. Marro and R. Dickman, *Nonequilibrium phase transitions in lattice models* (Cambridge Univeristy Press, Cambridge, MA, 1999).
[35] F. A. Williams, Journal of Loss Prevention in the Process Industries **21**, 131 (2008).

All three explosion limits of hydrogen oxidation are nonequilibrium critical points that terminate the coexistence of slow-burning and autoigniting dynamical phases.

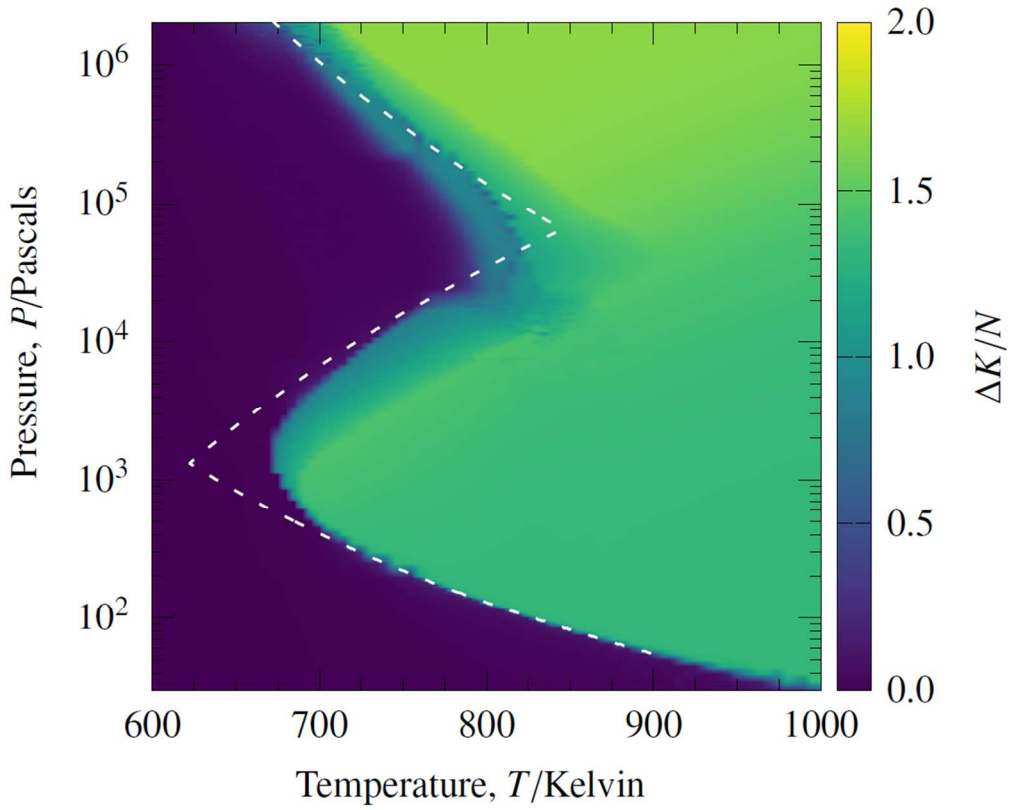

395x316mm (72 x 72 DPI)